The Principles of "Smart" Encapsulation: Using Additive Printing Technology for the Realization of Intelligent Application-Specific Packages for IoT, 5G, and Automotive Radar Applications

Bijan Tehrani, Ryan Bahr, and Manos Tentzeris
School of Electrical and Computer Engineering
Georgia Institute of Technology
Atlanta, GA, USA
Email:btehrani3@gatech.edu

Daniel Revier and Benjamin Cook
Kilby Labs
Texas Instruments
Dallas, TX, USA
Email: daniel.revier@ti.com

***Abstract*—This paper outlines the fundamental principles and processing characteristics of realizing application-specific "smart" microelectronic packages utilizing fully-additive inkjet and 3D printing fabrication technologies. Standard square encapsulants are 3D-printed directly onto dies as a comparison to traditional transfer molding encapsulant techniques. This standard encapsulant is expanded through the integration of microfluidic channels directly within an encapsulant as a fully-printed solution for thermal management and fluid sensing applications with an embedded silicon die. The process flow of fully-printed partial encapsulants with subsequent capping is outlined for the realization of 3D TMV interconnects, where measurements demonstrate a low-loss versatile 3D interconnection method with adequate matching and line loss below 0.46 dB/mm up to 40 GHz. Finally, a fully-printed partial die encapsulant with TMV interconnection is presented as a proof-of-concept for process verification.**

***Keywords*-encapsulation, microfluidics, millimeter-wave, interconnects, inkjet printing, 3D printing**

I. Introduction

Across the field of microelectronic packaging, industry standards for integrated circuit (IC) encapsulation rely on the process of epoxy molding, a process based on the thermal transfer molding of epoxy compounds for the protective sealing of an IC die. With the growing interest in the development of highly-integrated system-on-chip (SoC) and system-in-package (SiP) design schemes for emerging millimeter-wave (mm-wave) automotive radar, 5G wireless, and internet-of-things (IoT) applications, the focus of system design is continuing to broaden extend beyond the circuit-level and into the package-level. The standard epoxy molding processes involved with IC encapsulation currently offer minimal freedom for SiP integration, where the tooling and upscale required for diverse encapsulant functionality is unfeasible in a practical production-level setting.

Additive printing technologies such as 3D and inkjet printing are steadily emerging as an effective means to realize a variety of fundamental wireless components, including antennas, passives, and interconnects [1]. Additionally, microfluidic platforms that were typically restricted to microelectromechanical system (MEMS)-based fabrication technologies are finding a low-cost alternative through printing technology, however integration at the die level is still a work in progress [2], [3]. Similarly, stereolithography (SLA) 3D printing technology has proven to be effective at the component and even package level, however a balance must be found between low-cost methods and high resolution for mm-wave wireless solutions [4]–[9]. The introduction of highly-reconfigurable, low-cost additive printing methods to the field of IC encapsulation has the potential to enable a new level of on-demand functionality and intelligence to the design of microelectronic packages [10], [11]. Furthermore, this method of heterogeneous material integration, combining both printed metals and plastics, highlight the potential of printing technology to address SoC/SiP integration at a massive reconfigurable production scale.

This paper outlines the principles and fully-additive processes involved with the development of "smart" microelectronic encapsulants. The combination of inkjet and 3D printing technologies is used to realize encapsulants with integrated functionality, including microfluidic channels for thermal management and through-mold-via (TMV) interconnects for wireless SiP solutions. Finally, a proof-of-concept process verification is presented for the realization of a fully-printed die encapsulant with integrated TMV interconnects for emerging wireless applications in the mm-wave regime.

II. Materials and Processes

Inkjet printing involves the layer-by-layer deposition of electronic ink materials. For this effort, inkjet patterning is performed using a Dimatix DMP-2831 materials printer using 10 pL cartridges. Two electronic ink materials are printed with the inkjet system: a silver nanoparticle-based ink and a polymer-based dielectric ink. Metallic features are patterned using Sun Chemical EMD-5730, a silver nanoparticle-based ink with 40 wt% content loading capable of achieving a volume resistivity of 5–30 $\mu\Omega$ cm after thermal

2377-5726/18/$31.00 ©2018 IEEE
DOI 10.1109/ECTC.2018.00025

sintering (< 200 °C). Non-conductive films are patterned with a Microchem SU-8 polymer-based ink. The thickness of these printed dielectric films depends on the drop spacing and amount of printed layers or cartridge passes, which can range from 4 µm to beyond 100 µm [12]. Curing the SU-8 ink involves the following three steps. First a soft bake takes place on a hot plate from 60–110 °C over 10 min. Then UV crosslinking is performed with an exposure dependent on the thickness of the film. Finally, a hard bake takes place at 100 °C for 7 min to complete the curing process.

SLA 3D printing involves the selective photonic exposure and crosslinking of a UV-photosensitive material in a consecutive layer-by-layer fashion to realize a homogenous 3D object. Whereas the feature size of inkjet printing is determined by drop volume and ink spreading on a surface, the resolution of an SLA printing system is determined in the Z-axis by the build plate stepper motor and in the XY-plane by the source of maskless UV exposure system. 3D printing is performed using a custom LittleRP *bottom-up* SLA 3D printer with a 1080p Viewsonic PJD7828HD DLP projector operating as a 3000 lm maskless UV source. The projector is focused at a set distance from the vat of resin and target printing site to provide a resolution of approximately 40 µm in the XY-plane correlating to the size of a single pixel. The SLA material used in this effort is the Vorex (orange color) resin from MadeSolid, an acrylate-based photopolymer resin optimized for mechanical resilience, highlighting impact strength and toughness. As a balance between Z-axis resolution and printing speed, a 50 µm layer step height is used along with an exposure time of 3.5 s per layer. After the SLA printing is completed, the samples are submerged and agitated within two consecutive isopropyl alcohol (IPA) baths followed by a wash with deionized water to clean off any residual unexposed resin material. To complete the SLA process, a final post-print 1 J/cm^2 UV exposure is performed to ensure that the 3D-printed Vorex samples are fully cured.

III. 3D-Printed Encapsulant Solutions

The square encapsulant is a staple of traditional microelectronic packaging that serves the purpose of protecting the ICs and interconnects within from environmental elements, including physical stress, chemical degradation, and exposure to moisture or high humidity. The standard process for encapsulating microelectronic devices utilizes an epoxy mold compound (EMC) technique where preformed and preheated EMC material is injected into a mold featuring cavities and the package leadframe in a transfer molding fashion [13]. With the transfer molding process, the reconfigurability of an encapsulant is limited by the mold itself, where different encapsulant shapes require the machining of specific mold structures. Additive printing methods enable the fabrication of arbitrary 3D structures, which allow for the realization of microelectronic

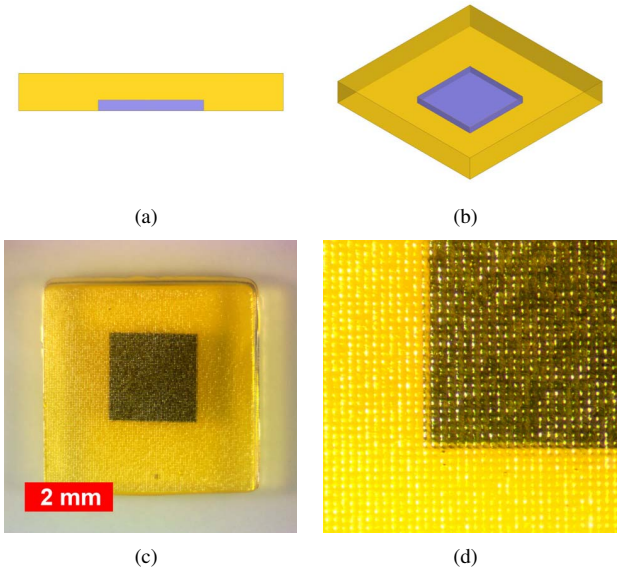

Figure 1. (a) Side and (b) perspective CAD models of 3D-printed square encapsulant. (c) Top and (d) detail micrographs of 3D-printed square encapsulant with silicon die.

encapsulants independent discrete molds for traditional EMC transfer molding techniques.

As an initial demonstration, a 3D square encapsulant is modeled and fabricated using the LittleRP 3D printer. Fig. 1(a–b) present 3D renderings of the proposed square encapsulant, where a silicon die is encapsulated with a 3D-printed dielectric material. The fabrication of the square encapsulant begins with the attaching of a 2×2×0.2 mm silicon dummy die to a 1 mm-thick glass slide using an inkjet-printed SU-8 polymer die attach. The glass slide behaves as a carrier substrate to facilitate the printing and post-print cleaning and curing profiles. The sample is attached to the metallic build plate of the 3D SLA printer using a small volume of Vorex resin and a subsequent UV exposure of 500 mJ/cm^2. A 5×5×0.5 mm square encapsulant model is aligned to the silicon die, where the printing of the model is set to begin at the top of the 200 µm-thick silicon die, yielding a total encapsulant height of 700 µm. 3D printing is then performed with the previously outlined process.

A fabricated sample of the 3D-printed square encapsulant is presented in Fig. 1(c–d). The detail micrograph in Fig. 1(d) highlights the inherent surface roughness of 3D structures fabricated with DLP SLA technology. This roughness corresponds to the pixels of the DLP projector used in the layer-by-layer exposure of the print, yielding a periodicity of approximately 40 µm and peak-to-peak roughness of less than 400 nm, which is a 25× reduction compared to typical fused deposition modeling (FDM) 3D printing [11].

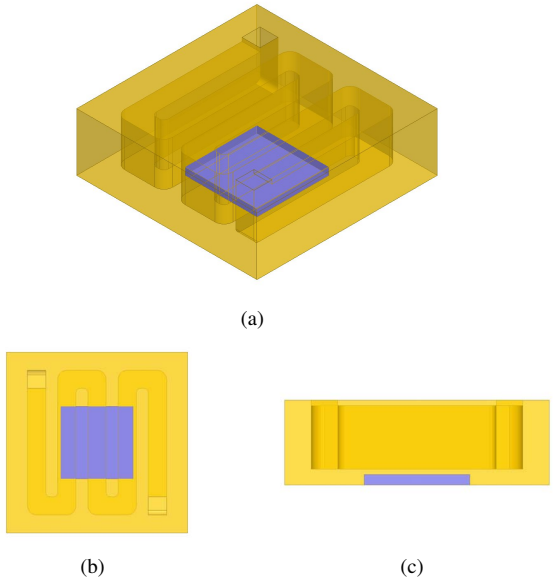

(a) (b) (c)

Figure 2. CAD model of 3D-printed microfluidic-integrated encapsulant with silicon die: (a) perspective, (b) top, and (c) side views.

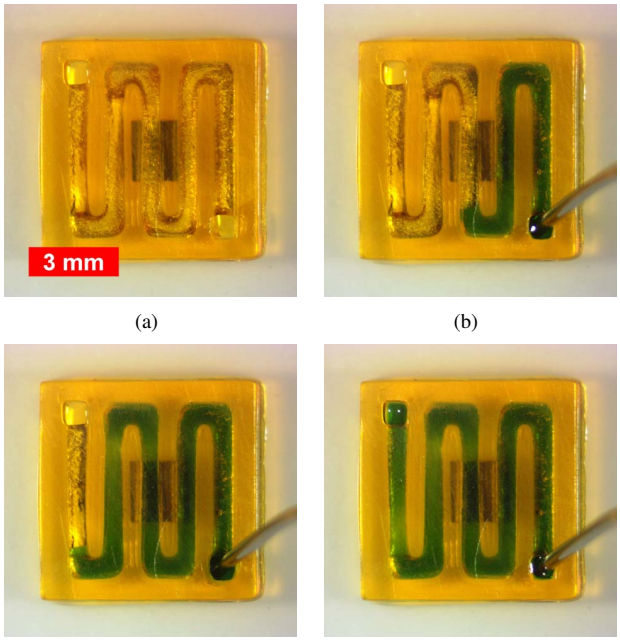

(a) (b) (c) (d)

Figure 3. 3D-printed microfluidic-integrated encapsulant with silicon die: (a) empty channel, (b–c) partially filled channel, and (d) completely filled channel.

IV. 3D-Printed Microfluidic-Integrated Encapsulant

As a maskless and moldless technology, 3D printing enables the design of arbitrarily-shaped and integrated microelectronic encapsulants with embedded IC dies. One such example of the capabilities of the technology for this application is the integration of microfluidic channels directly within an IC encapsulant. Package-integrated microfluidic channels can serve several purposes, including fluid-controlled circuit tuning, fluid component sensing, and liquid cooling for thermal management.

As a proof of concept demonstration, a 3D-printed microlfluidic-integrated encapsulant is designed for package-integrated thermal management. Fig. 2 presents a 3D microfluidic encapsulant model, featuring an inlet, outlet, and meandering channel atop the embedded die. The dimensions of the channel are designed to be 1.2×0.5 mm, yielding a full channel volume of approximately 12.8 µL. The $5\times5\times1.4$ mm encapsulant features a 100 µm-thick passivation between the embedded die and the microfluidic channel, however could be removed allowing for the fluid channel to interface directly with the die if desired.

Fabrication of the microfluidic-integrated encapsulant begins with the same die attach and glass carrier process outlined in the previous section. Printing and post-print cleaning take place with the addition of three cleaning steps to remove photopolymer resin from the microfluidic channels before the final UV curing. First, compressed air is directed to the inlet of the microfluidic channel to expel the uncured resin within the channels. Next, IPA is loaded into the channel followed by a submersion and sonication in IPA for 5 min. With all uncured resin expelled from the channel, the post-print UV cure takes place to complete the fabrication process.

A micrograph of a 3D-printed microfluidic-integrated encapsulant with silicon die is presented in Fig. 3(a). In order to validate the post-print channel cleaning process and verify the integrity of the channel, the 3D-printed encapsulant is loaded with water dyed with blue food coloring. Fig. 3(b–d) present the fluid loading process using a syringe directly inserted into the channel inlet. From the micrograph in Fig. 3(d), it is apparent that the microfluidic channel is successfully voided of photopolymer resin after printing and that overcuring leading to channel blockage is not an issue.

V. Printed Through-Mold Via (TMV) Ramped Interconnects

One of the most enabling features of utilizing additive printing technologies for microelectronic encapsulant design and fabrication is the concept of application-specific reconfigurability. Specifically for wireless packaging, industry standard EMC-based transfer molding techniques are limited to square encapsulants for the protection of the monolithic microwave integrated circuit (MMIC) die embedded within. However, through the development of arbitrarily-shaped encapsulants with 3D printing, functionality can be integrated into the microelectronic encapsulant in the form of antennas, passives, and other

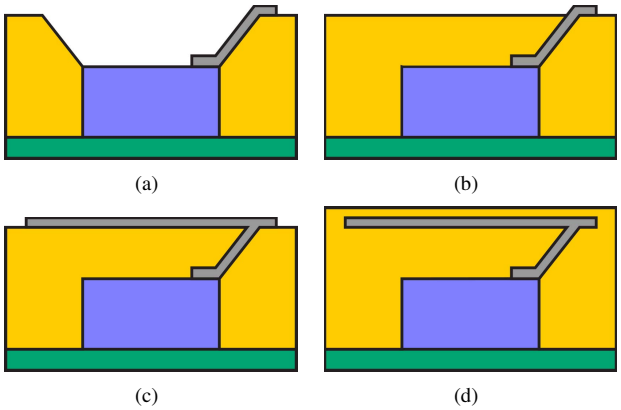

Figure 4. "Smart" wireless encapsulant process flow: (a) 3D print partial encapsulant with die and inkjet print sloped TMV. (b) Cap partial encapsulant with photopolymer resin leaving exposed TMV interconnecting to embedded die. (c) Inkjet print antenna, passive, or other SiP component. (d) 3D print final encapsulant.

components to achieve on-demand, unique SiP solutions for a variety of wireless applications.

Through-mold vias (TMVs) are essential components for the development of 3D "smart" encapsulants for wireless device packages [10]. Fig. 4 outlines the conceptual process flow for the fabrication of TMVs and SiP wireless encapsulants with 3D and inkjet printing. The efforts of this section are focused on the concepts presented in Fig. 4(a–b): printed ramped TMV fabrication and partial encapsulant capping.

A. TMV Fabrication with Partial Encapsulant Capping

To evaluate the feasibility of integrating TMV interconnects within a microelectronic encapsulant using additive printing technologies, a 3D test vehicle is designed featuring a partial encapsulant with sloped sidewalls. The sloped sidewalls bridge the top of the encapsulant to the bottom plane of the cavity 400 µm below with an angle of 30°. 3D printing fabrication of the test vehicle is performed on a glass carrier utilizing a 10 µm layer print height in order to reduce the discontinuous step height of the sloped sidewalls of the design. Fig. 5(a) presents a micrograph of the 3D-printed partial encapsulant test vehicle.

Before the inkjet printing of TMVs can take place, the roughness of the 3D-printed sloped sidewalls featured in the partial encapsulant test vehicle is investigated. An Alpha-Step D-500 surface profilometer from KLA Tencor is used to measure the stair-step discontinuities inherent with the SLA 3D printing technique. Fig. 6(a) presents the measured profile of the 3D-printed sloped sidewall using a 10 µm layer print height. The expected stair-step profile is apparent in the profilometer scan, where a step periodicity of approximately 40 µm is measured across the length of the 700 µm-length ramps corresponding to the size of the pixels used with the DLP SLA 3D printer. In an effort to reduce

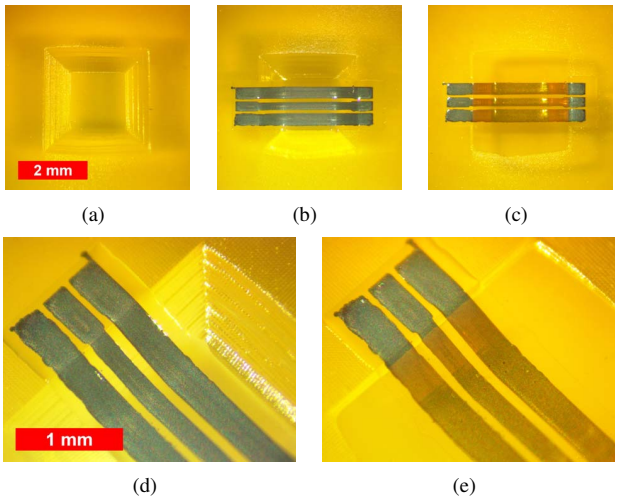

Figure 5. 3D-printed test vehicle for inkjet-printed TMV and partial encapsulant capping verification: (a) 3D-printed partial encapsulant, (b) inkjet-printed TMVs and (d) perspective detail, (c) capped TMV-integrated encapsulant and (e) perspective detail.

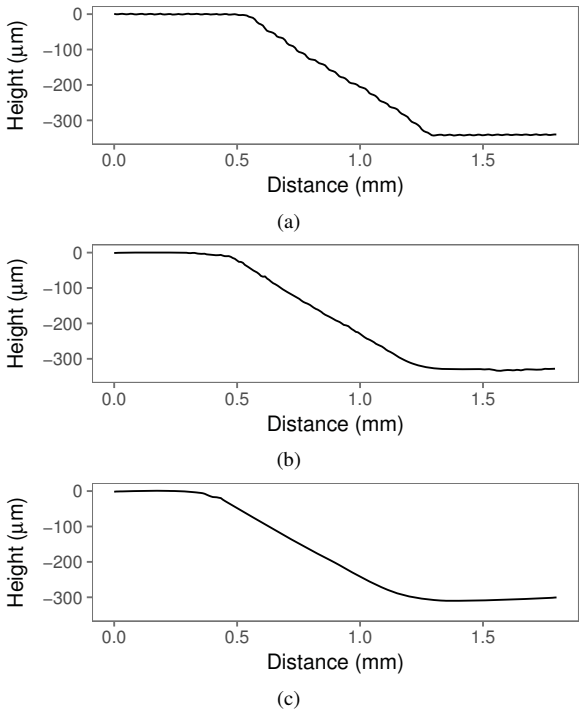

Figure 6. Surface profilometer scans of 3D-printed partial encapsulant sloped sidewalls with varying layers of printed SU-8 polymer passivation: (a) 0 layers, (b) 1 layer, (c) 2 layers.

the rough stair-step profile of the sloped sidewalls, SU-8 polymer ink is inkjet-printed across the partial encapsulant where the TMV interconnects will be subsequently printed. Fig. 6(b–c) present the measured surface profiles of the sidewalls with one and two printed layers with 20 µm drop spacing. With one layer of inkjet-printed SU-8 passivation,

the stair-step profile of the sidewalls is greatly reduced leaving only several discontinuities. Additionally, two layers of SU-8 passivation essentially eliminate all stair-step discontinuities, leaving a smooth transition from the top to the bottom planes of the partial encapsulant. From these results, it is determined that two layers of inkjet-printed passivation is adequate for realizing a smooth sidewall profile within a partial encapsulant.

With the surface profile continuity of the sloped sidewalls verified, TMV interconnects are fabricated using SU-8 polymer and silver nanoparticle inks. First, SU-8 polymer ink is printed to pattern the previously discussed passivation film yielding a thickness of approximately 10 µm. Curing of the SU-8 film takes place with the previously outlined processes including a UV exposure of 300 mJ/cm^2, followed by a 2.5 min UV-O_3 exposure to increase the surface energy of the printed film for subsequent silver ink printing. Next, 6 layers of silver nanoparticle ink printed to pattern coplanar waveguide (CPW) TMV interconnects featuring 50–60 µm gaps between the signal and ground conductors. The dimensions are slightly tapered when the CPW line enters the bottom of the partial encapsulant to account for the dielectric loading above the CPW in the final capped TMV design. Inkjet fabrication is completed with thermal sintering in an oven at 150 °C for 1 h. Fig. 5(b) and (d) present micrographs of the fabricated inkjet-printed TMVs on the 3D-printed partial encapsulant test vehicle. Following the inkjet-printing of the sloped TMVs, the partial encapsulant is then capped through the syringe deposition of Vorex photopolymer resin within the encapsulant cavity. Finally, the capped encapsulant undergoes a 3 J/cm^2 UV exposure and wash with IPA and deionized water. Micrographs of the fully-printed and capped TMV interconnects are presented in Fig. 5(c) and (e).

The S-parameters of the inkjet/3D-printed TMVs are measured from 10–40 GHz using an Anritsu 37369A VNA with Cascade Microtech ACP40-GSG-250 probes. Simulated and measured return and insertion loss are plotted in Fig. 7 for both partial encapsulant and capped printed TMVs. The return loss measurements exhibit improved matching for the capped samples, where maximum |S11| is measured to be −7.1 dB at 13.8 GHz for the partial encapsulant and −9.1 dB at 34.5 GHz for the capped encapsulant. Furthermore, the resonances present in the return loss measurements experience a shift from 27.8 GHz to 21.5 GHz due to the dielectric loading of the capping dielectric above the CPW line within the encapsulant. Insertion loss is measured to be 2 dB for both samples at 40 GHz, yielding a line loss of 0.46 dB/mm at 40 GHz for the 4.3 mm-length CPW line. Deviations between the experimental and simulated measurements are present for both sample topologies and are likely to be improved through the continued characterization of SLA photopolymers materials at Ka-band (26.5–40 GHz), where

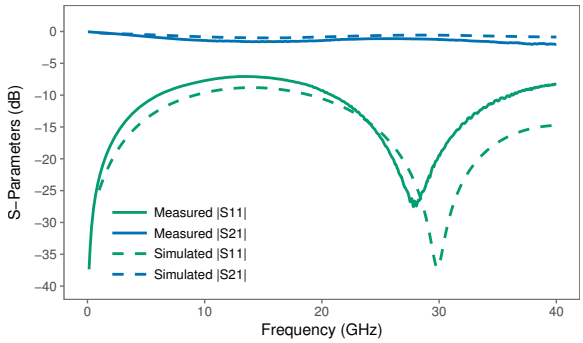

(a)

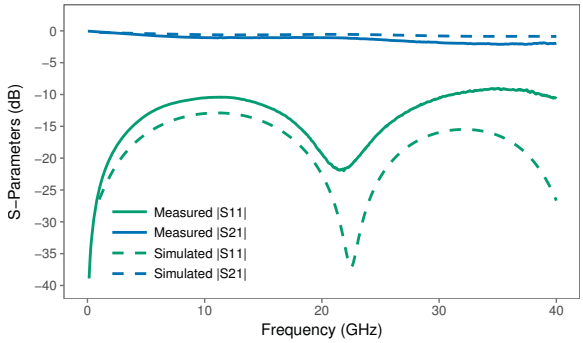

(b)

Figure 7. S-parameter measurements of simulated and fabricated inkjet/3D-printed TMVs (a) before and (b) after capping of the partial encapsulation.

parameters of loss tangent and relative permittivity of the Vorex material were extrapolated from E-band (60–90 GHz) characterization data for this effort [10]. Overall, the results of both of the fully-printed partially-encapsulated and capped TMV interconnects demonstrate the effectiveness of the technology for the fabrication of 3D package-integrated interconnects for wireless SiP applications.

B. Proof-of-Concept TMV Fabrication with Embedded Die

With the integrity of fully-printed embedded TMV interconnects outlined, focus is shifted to integration of these 3D and inkjet printing processes with an IC die for practical wireless SiP solutions. As a proof of concept, a partial encapsulant with ramped TMV interconnects and a silicon die is designed for process verification. A preliminary challenge is the alignment of the 3D partial encapsulant model of with a die to be packaged. Alignment between the two is crucial to avoid failure in the form of the 3D-printed model overlapping the fine-pitch interconnect pads present on IC dies and thus rendering them inaccessible for subsequent TMV interconnection. This challenge is mitigated through a pre-print alignment method within the SLA 3D printer, presented in Fig. 8. Once the sample is loaded into the 3D printer, the first layer of the 3D model to be printed is projected onto the die with a red layer

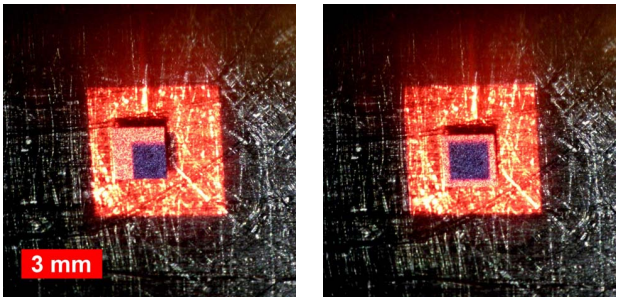

(a) (b)

Figure 8. Micrograph images of first-layer alignment method used for die encapsulation within an SLA 3D printer: (a) before and (b) after alignment.

color instead of the white layer color used in the standard printing process. The projection of a red colored layer does not contain significant UV spectrum, thus avoiding material polymerization while allowing for the accurate positioning of the 3D model onto the die. Once aligned, the layer color is returned to white and printing can begin.

The fabrication procedure for the fully-printed 3D TMV-integrated partial encapsulation with silicon die follows that of the previously outlined TMV test vehicle with the addition of the alignment methods outlined. Fig. 9 presents 3D models and micrographs of a fully-printed TMV-integrated partial encapsulant with a silicon die for process verification. The design of the TMVs with an encapsulated die feature a more pronounced taper in the dimensions of the CPW line over the die compared to the all-Vorex test vehical due to the higher dielectric constant of the silicon. The on-demand tuning of the TMV interconnect dimensions further highlights the application-specific capabilities of additive printing technologies, where designs can be reconfigured to desired performance parameters while maintaining an identical fabrication tooling and process flow.

VI. Conclusion

This paper outlines the fundamental principles and processing characteristics of realizing application-specific "smart" microelectronic packages utilizing fully-additive inkjet and 3D printing fabrication technologies. Standard square encapsulants are 3D-printed directly onto dies as a comparison to traditional transfer molding encapsulant techniques. This standard encapsulant is expanded through the integration of microfluidic channels directly within an encapsulant as a fully-printed solution for thermal management and fluid sensing applications with an embedded silicon die. The process flow of fully-printed partial encapsulants with subsequent capping is outlined for the realization of 3D TMV interconnects, where measurements demonstrate a low-loss versatile 3D interconnection method with adequate matching and line loss

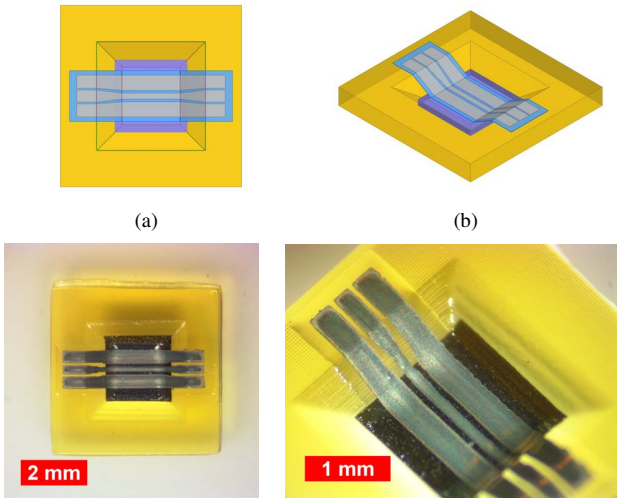

(a) (b) (c) (d)

Figure 9. Fully-printed 3D TMV-integrated partial encapsulant with silicon die: 3D model (a) top and (b) perspective view, fabricated sample (c) top and (d) perspective views.

below 0.46 dB/mm up to 40 GHz. Finally, a fully-printed partial die encapsulant with TMV interconnection is presented as a proof-of-concept process verification enabling fully-printed process-reconfigurable wireless packages for IoT, 5G, and automotive radar applications.

Acknowledgment

The authors would like to thank the Semiconductor Research Corporation (SRC) for their support with this work.

References

[1] S. A. Nauroze, J. G. Hester, B. K. Tehrani, W. Su, J. Bito, R. Bahr, J. Kimionis, and M. M. Tentzeris, "Additively manufactured rf components and modules: Toward empowering the birth of cost-efficient dense and ubiquitous iot implementations," *Proceedings of the IEEE*, vol. 105, no. 4, pp. 702–722, April 2017.

[2] W. Su, B. S. Cook, Y. Fang, and M. M. Tentzeris, "Fully inkjet-printed microfluidics: a solution to low-cost rapid three-dimensional microfluidics fabrication with numerous electrical and sensing applications," *Scientific reports*, vol. 6, p. 35111, 2016.

[3] M. Craton, M. I. M. Ghazali, B. Wright, K. Y. Park, P. Chahal, and J. Papapolymerou, "3d printed integrated microfluidic cooling for high power rf applications," in *International Symposium on Microelectronics*, vol. 2017, no. 1. International Microelectronics Assembly and Packaging Society, 2017, pp. 000 675–000 680.

[4] A. Joe Lopes, E. MacDonald, and R. B. Wicker, "Integrating stereolithography and direct print technologies for 3d structural electronics fabrication," *Rapid Prototyping Journal*, vol. 18, no. 2, pp. 129–143, 2012.

[5] T. Merkle, R. Gotzentzen, J. Y. Choi, and S. Koch, "Polymer multichip module process using 3-d printing technologies for d-band applications," *IEEE Transactions on Microwave Theory and Techniques*, vol. 63, no. 2, pp. 481–493, Feb 2015.

[6] N. T. Nguyen, N. Delhote, M. Ettorre, D. Baillargeat, L. L. Coq, and R. Sauleau, "Design and characterization of 60-ghz integrated lens antennas fabricated through ceramic stereolithography," *IEEE Transactions on Antennas and Propagation*, vol. 58, no. 8, pp. 2757–2762, Aug 2010.

[7] A. Khalil, N. Delhote, A. Pothier, A. Bessaudou, D. Baillargeat, S. Verdeyme, and H. Leblond, "Compact low loss alumina band-pass filter in ku band using layer-by-layer stereolithography technology," in *Microwave Symposium Digest, 2009. MTT'09. IEEE MTT-S International*. IEEE, 2009, pp. 1469–1472.

[8] R. A. Bahr, Y. Fang, W. Su, B. Tehrani, V. Palazzi, and M. M. Tentzeris, "Novel uniquely 3d printed intricate voronoi and fractal 3d antennas," in *Microwave Symposium (IMS), 2017 IEEE MTT-S International*. IEEE, 2017, pp. 1583–1586.

[9] W. Su, S. A. Nauroze, B. Ryan, and M. M. Tentzeris, "Novel 3d printed liquid-metal-alloy microfluidics-based zigzag and helical antennas for origami reconfigurable antenna trees," in *Microwave Symposium (IMS), 2017 IEEE MTT-S International*. IEEE, 2017, pp. 1579–1582.

[10] B. K. Tehrani, R. A. Bahr, W. Su, B. S. Cook, and M. M. Tentzeris, "E-band characterization of 3d-printed dielectrics for fully-printed millimeter-wave wireless system packaging," in *2017 IEEE MTT-S International Microwave Symposium (IMS)*, June 2017, pp. 1756–1759.

[11] B. K. Tehrani, S. A. Nauroze, R. A. Bahr, and M. M. Tentzeris, "On-package mm-wave fss integration with 3d-printed encapsulation," in *2017 IEEE International Symposium on Antennas and Propagation USNC/URSI National Radio Science Meeting*, July 2017, pp. 9–10.

[12] B. K. Tehrani, C. Mariotti, B. S. Cook, L. Roselli, and M. M. Tentzeris, "Development, characterization, and processing of thin and thick inkjet-printed dielectric films," *Organic Electronics*, vol. 29, pp. 135–141, 2016.

[13] N. Kinjo, M. Ogata, K. Nishi, A. Kaneda, and K. Dušek, "Epoxy molding compounds as encapsulation materials for microelectronic devices," in *Speciality Polymers/Polymer Physics*. Berlin, Heidelberg: Springer Berlin Heidelberg, 1989, pp. 1–48.